Monte Carlo Perturbation Analysis of Fuel Temperature Variations in The MCNP Model of The Annular Core Research Reactor [1]

Melissa Moreno [a], Danielle Redhouse [b], and Christopher Perfetti [c]

[1] *This paper was solely funded by Sandia National Laboratories Radiation Effects Science (RES) Campaign Mission. Sandia National Laboratories is a multimission laboratory managed and operated by National Technology & Engineering Solutions of Sandia, LLC, a wholly owned subsidiary of Honeywell International Inc., for the U.S. Department of Energy's National Nuclear Security Administration under contract DE-NA0003525.*

[a] *Graduate R&D Intern, Applied Nuclear Technologies, Sandia National Laboratories, P.O. Box 5800, MS 1146, Albuquerque, New Mexico 87185, USA, mmoreno@sandia.gov*

[b] *R&D S&E Nuclear Engineer, Modeling and Metrology, Sandia National Laboratories, P.O. Box 5800, MS 1146, Albuquerque, New Mexico 87185, USA, drredho@sandia.gov*

[c] *Associate Professor, Department of Nuclear Engineering, University of New Mexico, Albuquerque, New Mexico 87106, USA, cperfetti@unm.edu*

Monte Carlo Perturbation Analysis of Fuel Temperature Variations in The MCNP Model of The Annular Core Research Reactor

The Annular Core Research Reactor (ACRR) Monte Carlo N-Particle (MCNP) model is used by ACRR reactor operators and experiment designers at Sandia National Laboratories for a variety of computational calculations ranging from reactor kinetics parameter estimates, safety analyses, to experimental planning. To understand the dominant source of uncertainty within the MCNP model, perturbations in temperature were applied to individual ACRR MCNP fuel rods. Fuel rod temperatures were randomly sampled from a uniform distribution from operational temperatures to quantify temperature-related uncertainty effects. Stochastic mixing was used to blend the cross sections of the desired temperatures using the MCNP continuous and Thermal Neutron Scattering Treatment ($S(\alpha,\beta)$) libraries in ENDF/B-VII.1. This uncertainty analysis produced a 640 row by 640 column correlation and covariance matrix of the neutron energy spectra. Positive covariance was produced around the 1 MeV region and the 0.2 eV region. Correlation was found in the thermal and fast energy regions, but no correlation was observed in the slowing down energy region because interactions in this region are not dominated by fuel.

I. INTRODUCTION

Monte Carlo Perturbation Theory (MCPT) quantifies the uncertainty in a model or process by randomly sampling uncertain model parameters and examining their effects. This work performed a MCPT uncertainty quantification study with realistic boundary conditions to better understand the dominant sources of uncertainty within the Annular Core Research Reactor's (ACRR) Monte Carlo N-Particle (MCNP) model. The fuel temperature variation in the ACRR MCNP model was postulated as a primary source of uncertainty. This study randomly sampled the temperature within each ACRR fuel pin. A resulting 640-row by 640-column neutron energy spectrum covariance matrix and correlation matrix would be created to be

compared to the previously assumed covariance and correlation matrices to assess the uncertainty contributed by the fuel temperature variations.

Before proceeding with the core concepts of this project, it is necessary to state the assumptions made for this investigation. The first assumption is the previously assumed covariance matrix correctly represents the uncertainty in the ACRR spectrum from all variance sources. This work is derived from the work done by various scientists at SNL who developed a covariance matrix for the ACRR using a Monte Carlo perturbation method [1]. The second assumption is the simplified Uncertainty Quantification (UQ) method utilizing MCPT by the SNL scientists is sufficient to achieve a covariance matrix that accurately depicts the ACRR spectrum.

A. Background

Prior to discussing the methodology used in this project it is important to understand some background concepts: UQ, Monte Carlo Perturbation Theory (MCPT), neutron spectra, and the ACRR and its MCNP model.

1. UQ

When assessing systems using computer models, both aleatoric and epistemic uncertainty will be present [2]. These models propagate uncertainty based on changes to the input parameters, and the impact of such variations can be determined in the output through data analysis tools [3]. In this project, nuclear data uncertainty is introduced to the ACRR MCNP model via random input temperature variations. The propagation of uncertainties is assessed with a covariance matrix which uses the outputs of the model to display if the data has positive, negative, or no correlation.

a) Monte Carlo Method and Perturbation Theory

The MCNP code employs the Monte Carlo statistical sampling technique to simulate histories of individual neutrons and to infer the average behavior in radiation transport problems. The MCPT technique can be applied to MCNP simulations by introducing small random changes to input parameters and analyzing the resulting distribution of quantities of interest. In neutron transport, uncertainties in the reactor geometry, material composition, and material temperature can affect important quantities such as the neutron multiplication factor and the neutron spectrum [3].

b) Covariance Matrix

When calculating the uncertainty of a continuous multivariable system, the covariance defines the linear relation between two random variables in that system. To build a covariance matrix at least two random variables and two sets of measurements are required, and the covariance matrix can have as many variables and sets of measurements as needed. Increasing the sets of measurements will improve the resolution of the matrix, and the size of the covariance matrix will be dictated by the number of random variables.

An example of a covariance matrix plot is shown in Figure 1. This example is the previously assumed covariance matrix for the neutron energy spectrum in the ACRR, built using physics-based methods [4]. The previously assumed covariance matrix shows variance produced in the cold neutron region, the thermal neutron region, some relation in the slowing down region, and the fast neutron region.

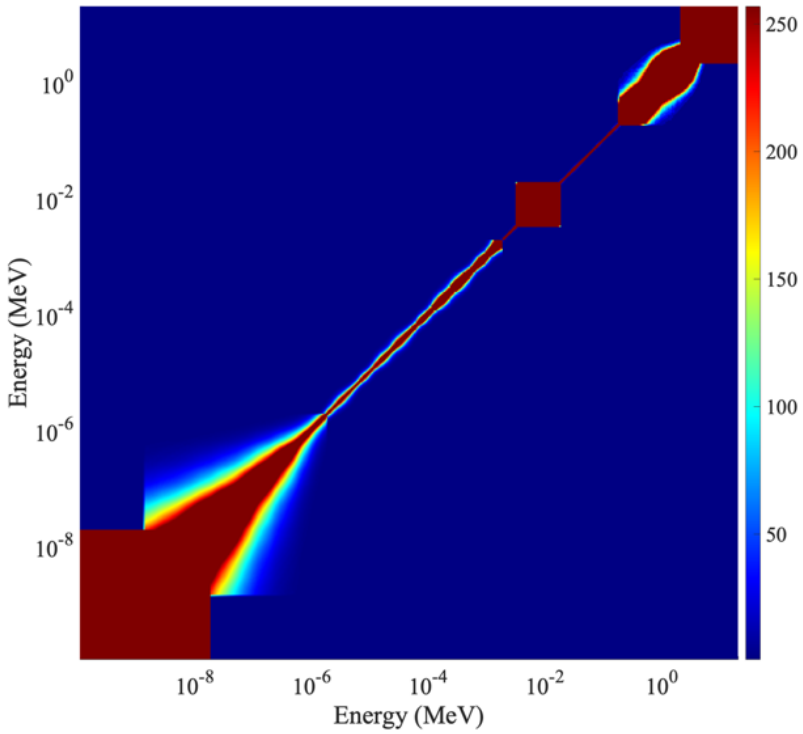

Figure 1. Previously assumed covariance matrix of the neutron energy spectrum of the ACRR.

c) Correlation Matrix

Correlation is calculated using the covariance, and it provides a tool to assess the magnitude and direction of the linear relationship between two variables. Equation (*1*) shows how to calculate the correlation coefficient, where the σ_x and σ_y terms are the standard deviations for data set x and y. The value of $corr(x, y)$ can range from 1 for perfectly correlated data to -1 for perfectly anti- correlated data [5].

$$corr(x,y) = \frac{cov(x,y)}{\sigma_x \sigma_y} \tag{1}$$

If the correlation coefficient is close to ±1, a correlation exists, and the values will lie close to a straight line in either the positive or negative direction. If the correlation lies close to 0, the values are linearly uncorrelated and will not fall on a straight line.

The correlation matrix shown in Figure 2 is the previously assumed correlation matrix for the neutron energy spectrum in the ACRR calculated using the previously assumed covariance matrix [4]. This plot shows the same positive correlation between the cold neutron region, thermal neutron region, some relation in the slowing down region, and the fast neutron region seen in the previously assumed covariance matrix. In addition, this plot shows how strong the correlation is between the different neutron energy regions, dark red being the most positively correlated, and green indicating no linear correlation between those energy regions.

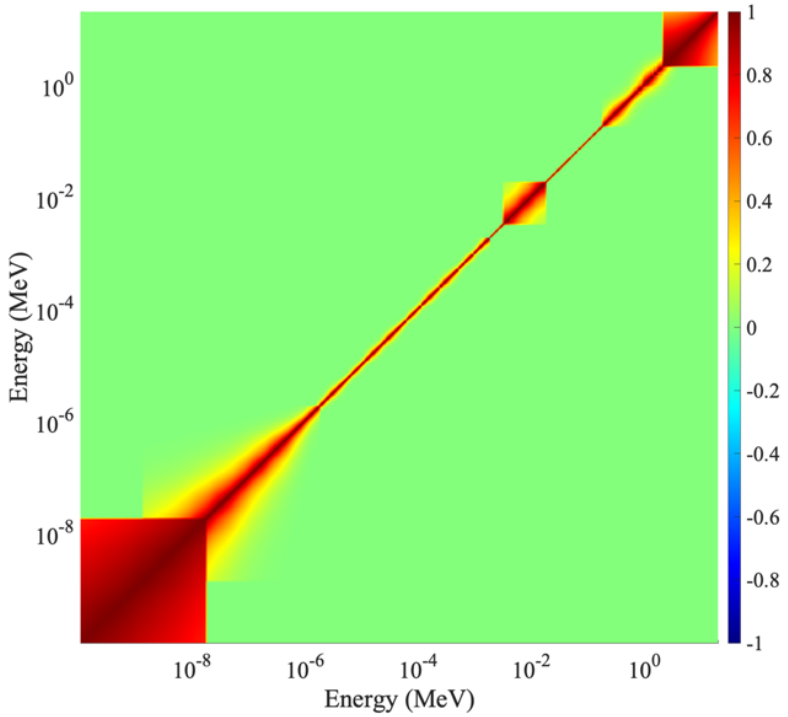

Figure 2. Previously assumed correlation matrix of the neutron energy spectrum of the ACRR. Strong positive correlation (red) exists in the cold neutron region (0.0 eV – 0.025 eV), the thermal neutron region (0.025 eV to 1 eV), to an extent in the slowing down region (1 eV – 1 MeV), and in the fast neutron region (1 MeV – 20 MeV).

The previously assumed covariance and correlation matrices shown in Figure 2 and Figure 3, were built using parametric equations based on reactor physics that calculated the neutron spectrum in three sections: thermal, epithermal, and fast region. The Monte Carlo method was used to run calculations for the previously assumed matrices to be built, which made it computationally expensive. The previously assumed matrices are used for reactor characterization providing scientists with conversion values used in experiments.

2. Annular Core Research Reactor (ACRR)

The ACRR provides unique capabilities used to perform a wide variety of experiments at Sandia National Laboratories (SNL). ACRR features include: a large, dry central cavity, an epithermal neutron flux, large pulsing capabilities, and the Fueled-Ring External Cavity-II (FREC-II) [6]. The ACRR is a pool-type research reactor with pulse, transient, and steady-state capabilities, and Figure 3 shows the ACRR and the FREC-II during a pulse operation. The ACRR has 236 fuel rods featuring uranium dioxide-beryllium oxide (UO2-BeO) similar in size and shape to TRIGA fuel but designed to have a larger heat capacity, which accommodates larger pulsing capabilities. The ACRR can operate in steady-state mode up to 2 MW, can provide power pulses up to 250 MJ of energy release with a 6 ms full-width at half maximum (FWHM), and can operate in transient mode up to 300 MJ [6]. The maximum temperature in the fuel at the time the transient rods reseat into the reactor is approximately 1248 K.

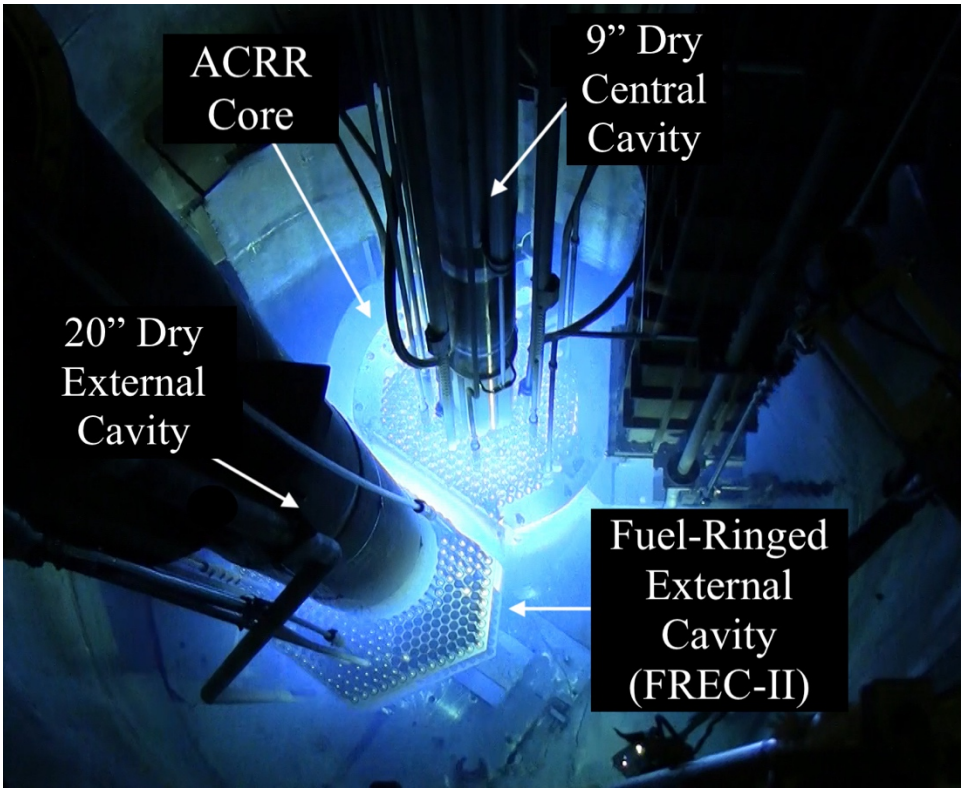

Figure 3. Pictured is the ACRR and FREC-II during a pulse operation. In the top center of the picture is the ACRR core and protruding from it is the 9” dry central cavity. In the bottom left of the image is the FREC-II core with its 20” dry central cavity. The surrounding medium for the core is 64,000 liters of deionized water [6].

The ACRR is typically used to perform irradiation testing where a high neutron fluence is required within a short period of time. The ACRR experiments include radiation damage in materials testing, nuclear fuels testing, space nuclear thermal propulsion testing, and medical isotopes production.

A typical MCNP-generated 640-group neutron energy spectrum lethargy fluence for the unmoderated central cavity is shown in Figure 4. Figure 4 provides a depiction of the lethargy fluence over the neutron energy range from 1×10^{-4} eV to 20 MeV showing the Maxwellian thermal peak, slowing down 1/E region, and the Watt fission peak [7]. About 46% of the ACRR

neutron fluence is above 100 keV and about 58% is above 10 keV. The energy fluence peaks at about 1 MeV and the thermal energy peak occurs at approximately 0.07 eV. At the radial centerline of the ACRR central cavity, and the axial centerline of the fuel, the neutron fluence is about $2.0 \times 10^{13}\ n/cm^2$ per MJ of reactor energy [6].

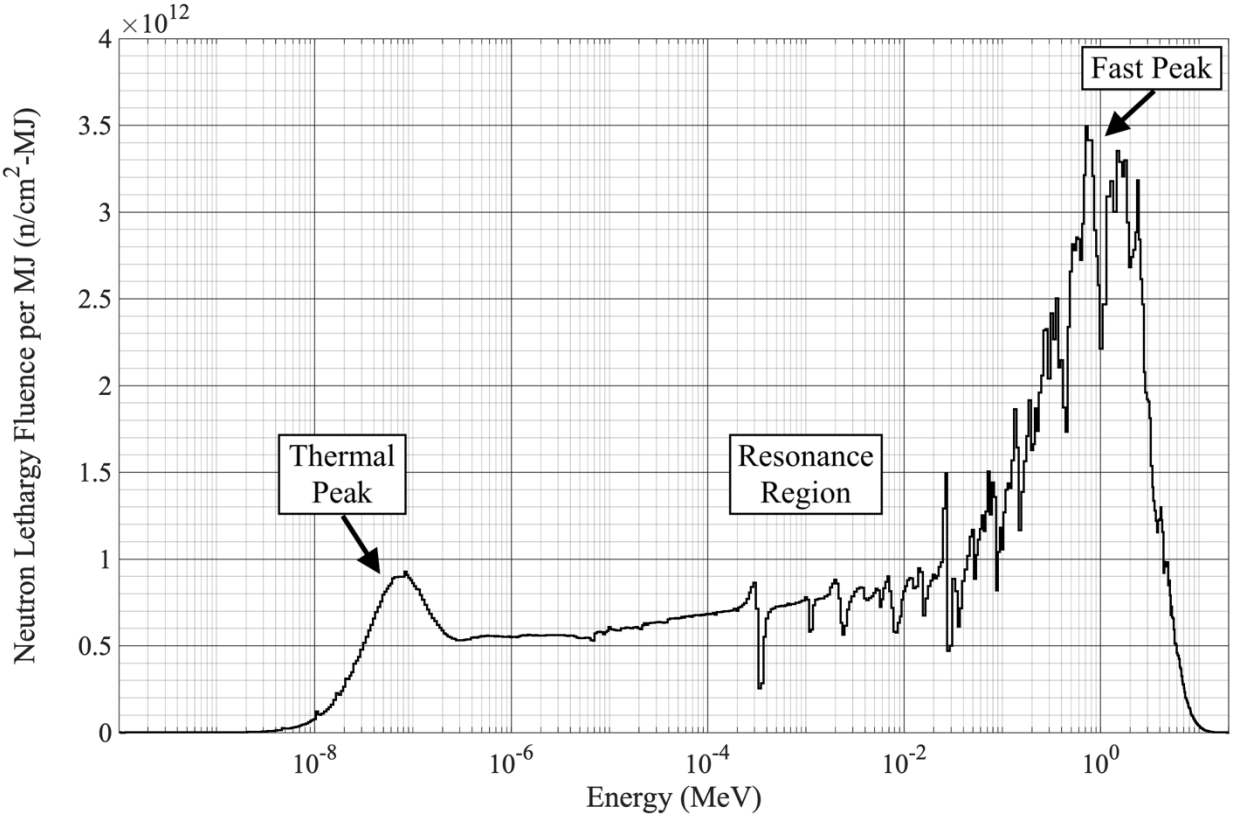

Figure 4. ACRR 640-group neutron energy fluence per MJ with thermal peak, resonance region, and fast peak indicated. The 640-group neutron energy fluence per MJ is plotted in linear-logarithmic scaling.

a) ACRR MCNP Model

This project analyzed the benchmarked ACRR MCNP model with FREC-II decoupled from the system shown in Figure 5; studies of ACRR and FREC-II coupling were outside the

scope of this project [8]. The average neutron multiplication factor (k_{eff}) for the benchmarked ACRR MCNP model is 1.000146 ± 0.001313 [8]. The Free-Field ACRR (ACRR-FF) MCNP configuration was used, which means that no central cavity buckets were included in this model. The MCNP model contains the main components of ACRR, including: the central cavity, radiography tube, positioning pedestal and fuel rods. Most of the ACRR model utilizes the ENDF/B-VII.0 and ENDF/B-VII.1 nuclear data libraries [9].

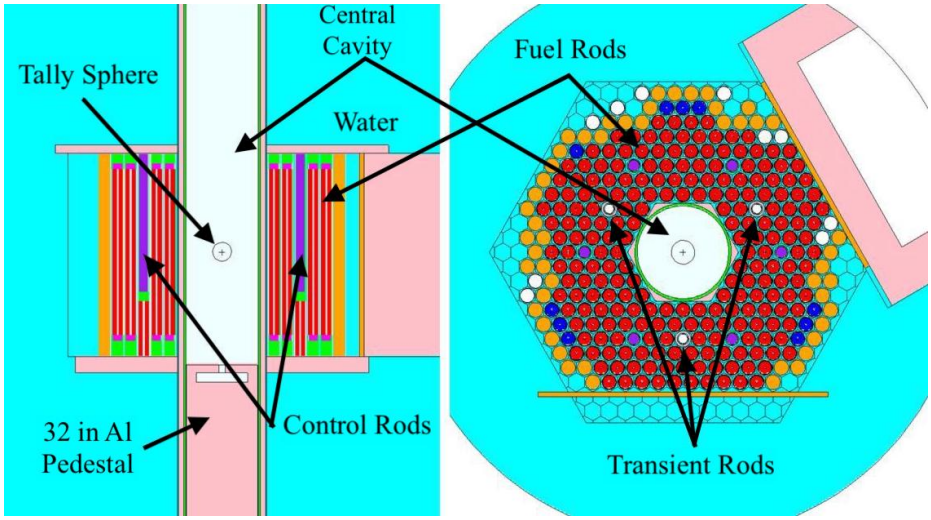

Figure 5. The MCNP ACRR benchmark model is shown in XY and YZ plane views of the core. The fuel rods are indicated in red, transient rods are identified as white, and the control rods are designated as purple. The nickel rods and nickel plate are shown in orange. The 9" dry central cavity and the tally sphere are also seen in this figure in the central light-gray region at the center of the core. The tally sphere is 6 cm in diameter. The tally sphere is located at the center of the cavity and filled with air at standard temperature and pressure.

II. METHODOLOGY

The programs and languages used to complete this project were MCNP 6.3 [3], SCALE (KENO VI) [10], MATLAB [11], and Python [12]. This section will review the implementation

of temperature perturbations into MCNP, including the temperature distributions, stochastic mixing, building the MCNP inputs, post-processing of the resulting data, and the required number of particles in each MCNP simulation.

A. Random Uniform Temperature Distribution

The fuel pin temperatures were randomly sampled from a uniform distribution between 293.6 K and 1200 K. The maximum fuel temperature of 1248 K [13] was not included in the sample space because 1200 K is the maximum temperature the S(α,β) libraries list for BeO (part of the fuel materials) [14]. This process was repeated 236 times in each case to ensure the sampling space for each temperature was unique. To confirm the desired range was sampled correctly in the solution space the temperatures from all the cases, about 26,000 different temperatures, were used to confirm the solution space quantitatively and visually was uniform and not biased to any region within the energy range.

B. Stochastic Mixing in MCNP

Traditional MCNP would require each temperature randomly selected to have a different cross section for each material in the fuel. This means thousands of unique cross sections would be needed. Instead of building cross sections for each temperature, a method called stochastic mixing was used. The stochastic mixing method uses the boundary temperatures of a range to approximate a desired discrete temperature within this range [15]. The percentages required from each temperature are calculated using Equation (2) and Equation (3). The terms x and y are the fractions of the temperature and terms a, b and c are the different temperatures.

$$x + y = 1 \tag{2}$$

$$ax + by = c \tag{3}$$

MCNP Version 6.2 does not support stochastic mixing of the S(α,β) thermal neutron scattering libraries, only of the free-gas cross section libraries. MCNP Version 6.3 supports this feature and uses the weight fractions specified in the material cards (*M*) to mix the S(α,β) libraries to the temperature specified in *MT* cards. An advanced issue of MCNP 6.3 was used in this work but is currently a pre-released version.

1. Stochastic Mixing Implementation Example

To show how stochastic mixing would look in the MCNP material section, Figure 6 has an example of how BeO was stochastically mixed to a temperature of 864 K. The *M* and *MT* cards are labeled as *M1* and *MT1* identifying them as material 1, and they must always have the same numerical post-script for the same material.

```
MT0     be-o.23t     4009.81c      $600 K
        be-o.27t     4009.83c      $1200 K
        o-be.23t     8016.81c      $600 K
        o-be.27t     8016.83c      $1200 K
M1      4009.81c     - 2.01E-01    4009.83c    - 1.59E-01
        8016.81c     - 3.58E-01    8016.83c    - 2.82E-01
MT1     be-o.23t     be-o.27t      o-be.23t    o-be.27t
```

Figure 6. MCNP input sample for stochastic mixing of BeO at 864 K. This figure shows the MT0 card which list all the cross sections required for stochastic mixing specific temperatures. The M1 card defines the temperature-fraction and mass-fraction product for each cross section and uses these to stochastically mix the continues-energy neutron cross sections. The MT1 card

shares this temperature-fraction and mass-fraction product listed in the M1 card to calculate the desired temperature and stochastically mixes the S(α,β) neutron cross sections.

The *MT0* specification card section of Figure 6 is unique to the stochastic mixing of S(α,β) in MCNP 6.3. This *MT0* card must be printed before the first *MT* stochastically mixed card. The *MT0* lists all the S(α,β) library identifiers used to stochastically mix material temperature in MCNP. In the *M1* section of Figure 6, the isotope identifying numbers are printed twice. The first column of isotopes references the lower temperature library signified with .81c for 600 K, and the second column of isotopes reference the higher temperature library using the .83c for 1200 K. Both library identifiers must be present when stochastically mixing nuclear data libraries. The total mass fraction of BeO is split up between the two isotopes into Be and O. The beryllium mass fraction is then separated into two using the temperature fractions required to mix the desired temperature. These mass fractions are then paired up with the correct temperature cross section identifiers. The same procedure is done for oxygen.

If the mass fractions for the low and high temperature are added, the total would be 0.36 for beryllium in the oxide and 0.64 for oxygen in the oxide. The *MT1* card also lists two library identifiers that match the temperatures for the *M1* card. In this instance .23t belongs to 600 K, and .27t belong to 1200 K as shown in Figure 6.

2. Stochastic Mixing Verification

After the implementation of stochastic mixing in MCNP, a three-step verification process was required for stochastic mixing before it was to be used in this paper:

Step 1) compares k_{eff}'s acquired using MCNP libraries versus k_{eff}'s acquired by stochastically mixing the MCNP libraries.

Step 2) compares stochastic mixing using two temperature libraries, versus stochastic mixing using three temperature libraries.

Step 3) compares stochastic mixing using MCNP libraries versus problem-dependent Doppler Broadening in SCALE (Version 6.2.3). Both MCNP and SCALE used the same ENDF-VII.0 and ENDF-VII.1 libraries in this analysis.

Step 1) showed stochastic mixing is sensitive enough to affect the k_{eff} from a small temperature variation at three significant figures. Step 2) showed stochastic mixing using three temperatures was acceptable with 99% confidence (3σ). Step 3) required an ACRR fuel rod to be modeled in both MCNP and SCALE. These input files were run using the original size of the fuel rod shown in Figure 7.

Shown are the SCALE and MCNP XY and YZ plane views of an ACRR fuel rod. Included are the central void in both models, the fuel indicated in blue (SCALE) and pink (MCNP), and the cladding is green (SCALE) and yellow (MCNP). The BeO plugs are darker-yellow above and below the fuel in both models and the stainless-steel plugs are green (SCALE) and yellow (MCNP) above and below the BeO plugs. For both models an infinite reflective water boundary was applied and it is shown as the hexagonal boundary red (SCALE) and cyan (MCNP).

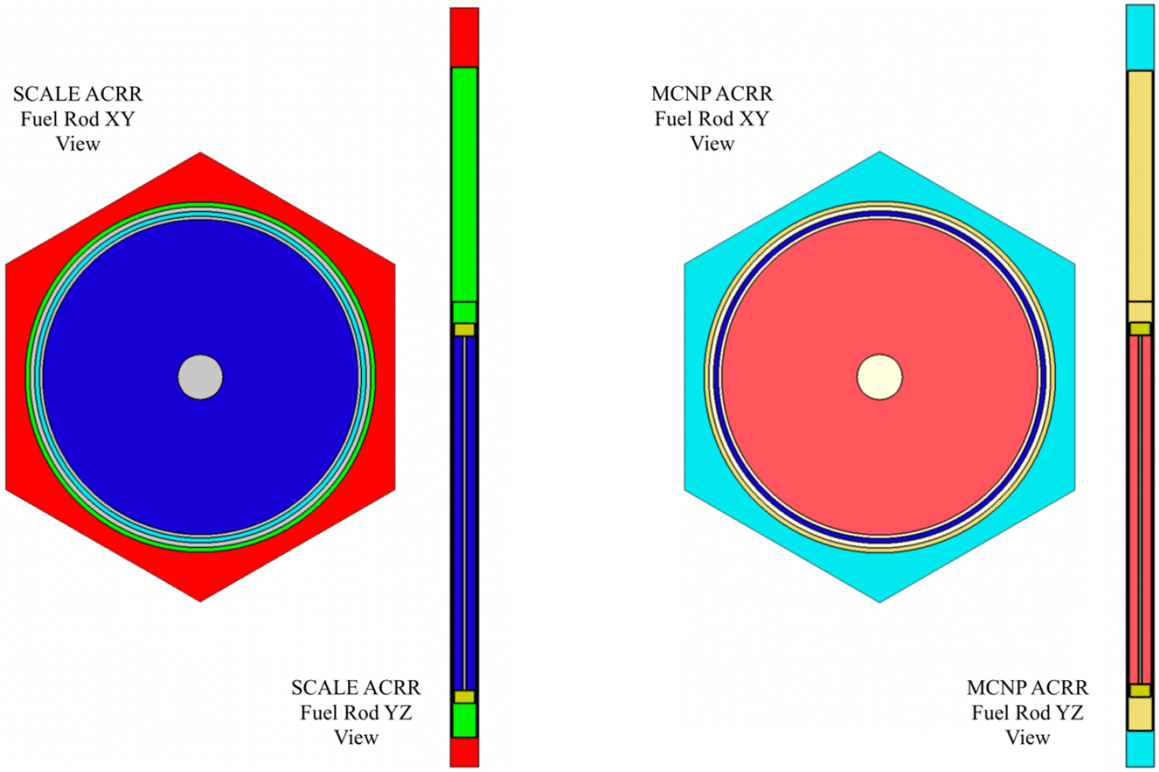

Figure 7. In the figure both the XY and YZ view of the fuel rod are shown. The XY view shows the central void, the surrounding fuel, niobium cups, the stainless-steel cladding, and water enclosed by a hexagonal boundary. The YZ view shows the central void, the surrounding fuel, the upper and lower BeO plugs, the upper and lower stainless-steel plugs, the stainless-steel cladding, and the surrounding water.

Like MCNP, the data libraries in SCALE contain only a limited selection of temperatures per isotope and the SCALE parameter **DBX** provides problem-dependent temperature Doppler broadening corrections. In SCALE, the thermal scattering data can also be Doppler broadened. Problem-dependent Doppler broadening in SCALE has the following options:

DBX=0 does not Doppler broaden, but instead selects the nearest temperature,

DBX=1 performs problem-dependent Doppler broadening for the resolved and unresolved resonance ranges, and

DBX=2 perform corrections for the S(α,β) thermal scattering data.

For this evaluation **DBX**=2 was selected. ACRR fuel rod runs were performed at different temperatures in both MCNP, and SCALE. Ten temperatures were analyzed and their k_{eff}'s were extracted and are shown in Figure 8. Since the amount of fuel in one rod is not enough to produce a significant k_{eff}, both MCNP and SCALE models of the fuel rod were run using the outer surface as an absolute reflector. The reflective surface did not allow the particles to escape the system, so the k_{eff}'s were much higher, giving a better assessment of the mixed temperatures the k_{eff} values for SCALE were slightly greater than the k_{eff} values calculated using stochastic mixing in MCNP, as shown in Figure 8. The accepted difference between k_{eff}'s produced in MCNP versus SCALE (KENO VI) is less than 1% [16], and after performing a difference of the sum of squares on the data produced by SCALE doppler broadening and stochastic mixing in MCNP, the uncertainty between the k_{eff}'s was found to be about 0.88%.

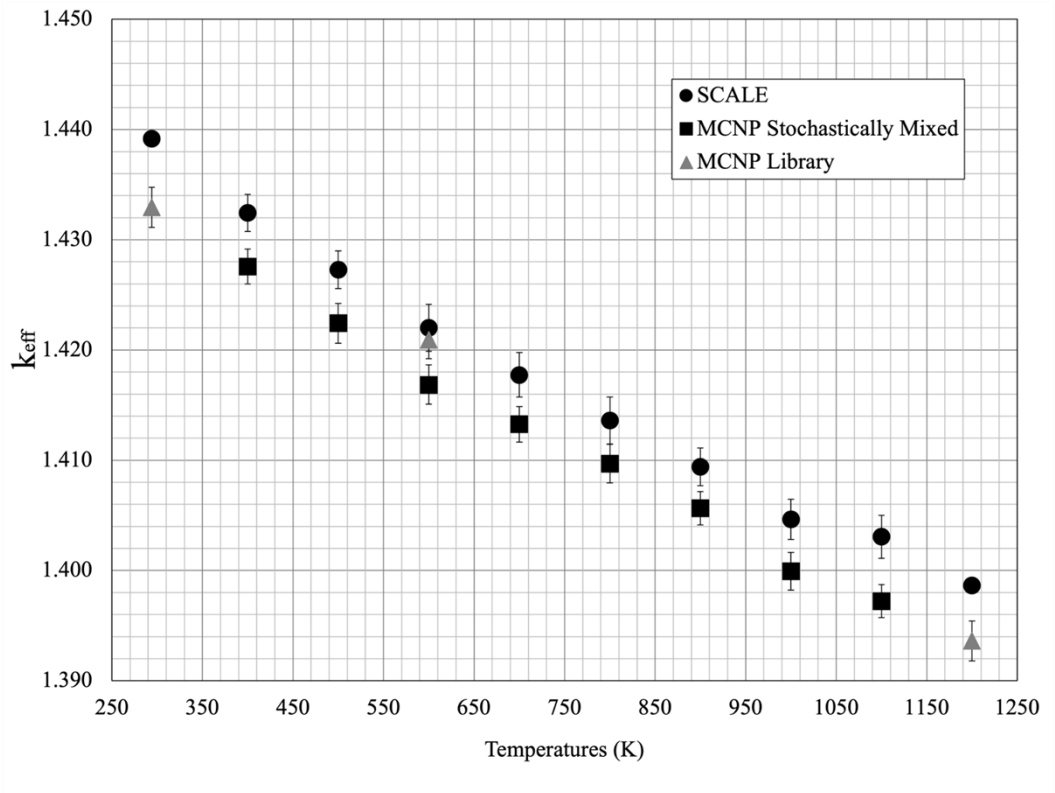

Figure 8. Verifying that MCNP's stochastically mixed k_{eff}'s match SCALE (KENO VI) problem-dependent Doppler broadened $k_{eff.}$ All data points lie within error bars representing an 0.88% uncertainty.

Verification Steps 1), 2), and 3) show stochastic mixing adequately approximates temperatures in MCNP and verified the decision to use stochastic mixing in this study.

C. ACRR MCNP Printing

Instead of having to modify or build hundreds of ACRR MCNP input files manually, a Python script was written to carry out this process. Python is used to make updates to universe numbers, cell numbers, material numbers, temperatures, weight fractions, and then prints everything into an MCNP ACRR input file format. Each fuel rod is assigned a randomly sampled temperatures from an operational range. Each temperature is considered a different material in

MCNP, resulting in an ACRR model with 236 unique material descriptions (i.e. plotted as different colors) as shown in Figure 9, when plotted using XQuartz. These files are referred to as multi-temperature cases.

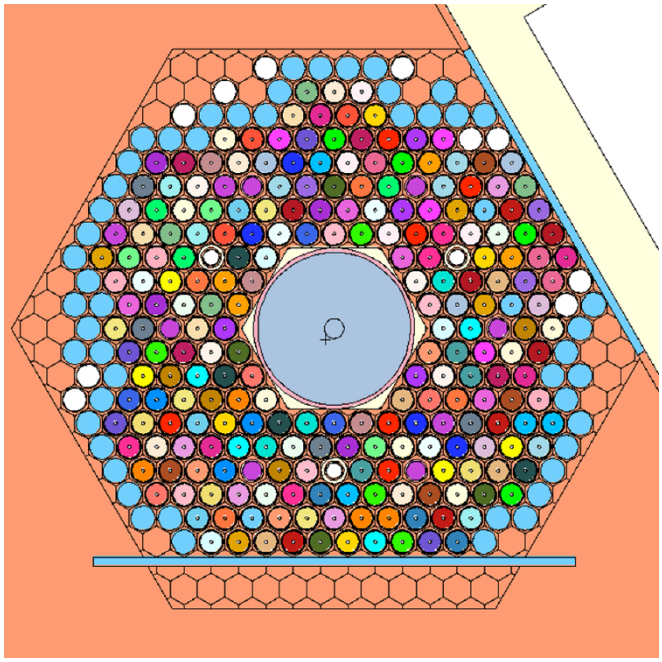

Figure 9. The XY plane view of a multi-temp ACRR MCNP model. The transient rods (white), Ni rods, and Ni plate are unchanged (light blue). The fuel rods, control rods, and safety rods have different colors indicating different temperatures.

D. ACRR MCNP Case Testing

At first, a covariance matrix built using cases with 20-million particles was assessed and the standard deviation precision of the 640-group neutron energy spectrum was not acceptable. After evaluating three benchmarked ACRR MCNP runs at room temperature (293.6 K) with: 20-million, 2-billion, and 20-billion total particles, shown in Figure 10; it was decided that 2 billion particles were ideal for both the 640-group neutron energy spectrum precision and the length of the run.

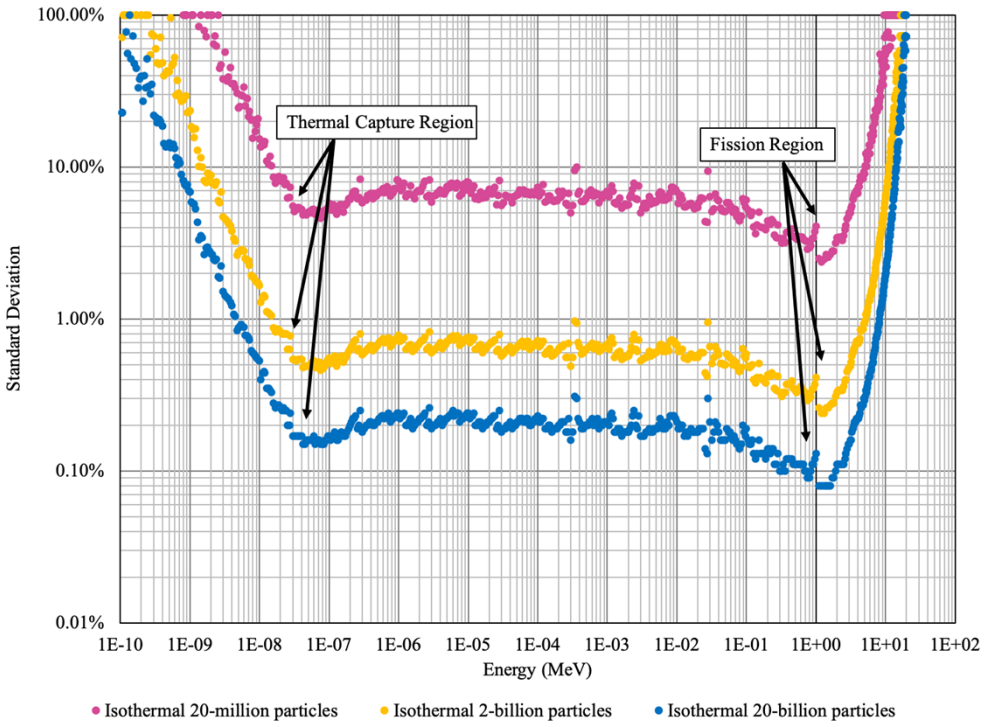

Figure 10. Standard deviation comparison between 20-million, 2-billion, and 20-billion particles. These comparisons were done using an isothermal (293.6 K) benchmarked model tested with different number of particles. All three follow the same trend, and the standard deviation decreased with number of particles as expected by $1/\sqrt{N}$ correlation. The reduction in the standard deviation between 2-billion particles and 20-billion particles was not efficient enough to warrant the use of 20-billion particles per MCNP input file.

MCNP 6.3 was available for local usage only when this project took place, so local clusters were used at Sandia to run all the cases. It was determined 110 cases were sufficient after performing a convergence test with each case's total neutron fluence per MJ. After 40 cases, the average neutron fluence per MJ starts convergence on an average of 2.0351×10^{13} $n/cm^2 - MJ$, which corresponds to the benchmarked axial centerline neutron fluence of about 2.0×10^{13} $n/cm^2 - MJ$. These 110 ACRR MCNP multi-temp cases using 2-billion particles

each were simulated, and the results of these simulations were used to generate a 640 by 640 correlation and covariance matrix.

III. RESULTS

The 640-group neutron energy spectra for all 110 cases were converted to fluence per MJ and plotted against the isothermal MNCP case results at 747 K. The temperature 747 K corresponds to the average of the multi-temp temperature distribution. The 747 K isothermal spectrum agrees with the multi-temp spectra across all energies as seen in the zoomed-in section (8x) of Figure 11. In this figure the 640-group neutron energy spectra for all the cases had similar shapes.

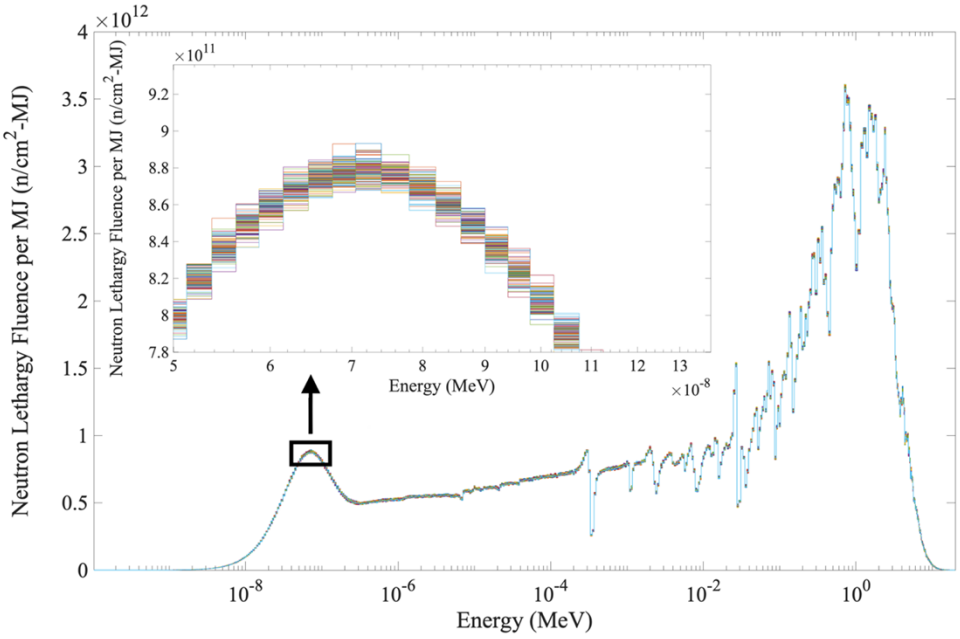

Figure 11. Displayed are all 110 multi-temp and isothermal (747 K) spectra in units of Fluence per MJ. The cases followed the same trend as the isothermal (747 K). This isothermal (747 K) case confirms the uniform distribution of temperatures produced a spectrum all the other cases varied about as expected.

The raw data was used to build the covariance matrix of the 640-group neutron energy spectra for 2-billion particles, as shown in Figure 12. This covariance matrix identified shared variance with the previously assumed covariance matrix around the fast neutron energy region at 1 MeV, and the thermal neutron region at 0.2 eV.

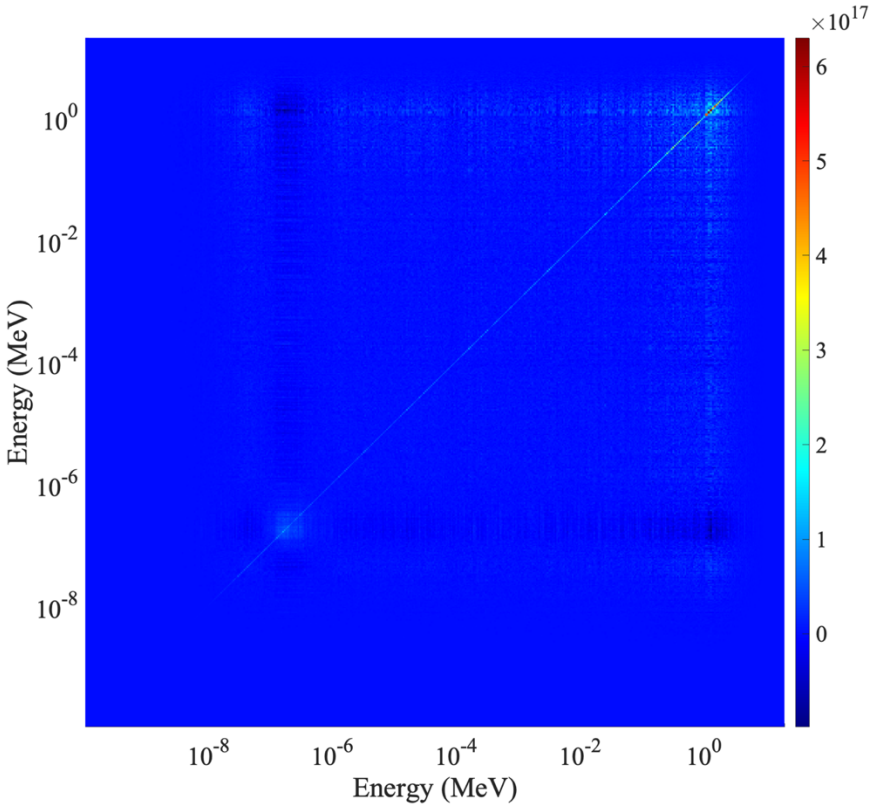

Figure 12. Shown is the covariance matrix for 640-group neutron energy spectrum based on the 110 multi-temp cases. Variance is produced in the fast and possibly the thermal region. Negative variance is observed in the fast to thermal correlated regions.

The raw data was used to build the correlation matrix plot for the 640-group neutron energy spectra, as shown in Figure 13. This correlation matrix observed correlation in the region around 1 MeV and the region around 0.2 eV, which corresponds to the fast neutron and thermal neutron energy region respectively, which also corresponds to the shared

variance identified in the covariance matrix. Insignificant correlation is observed within the slowing down region. Negative correlation bands exist within the thermal energy region showing inverse correlation, corresponding to the balance in the epithermal and fast regions. Since data smoothing was not used on the raw data, this explains the horizontal and vertical lines seen throughout the figure.

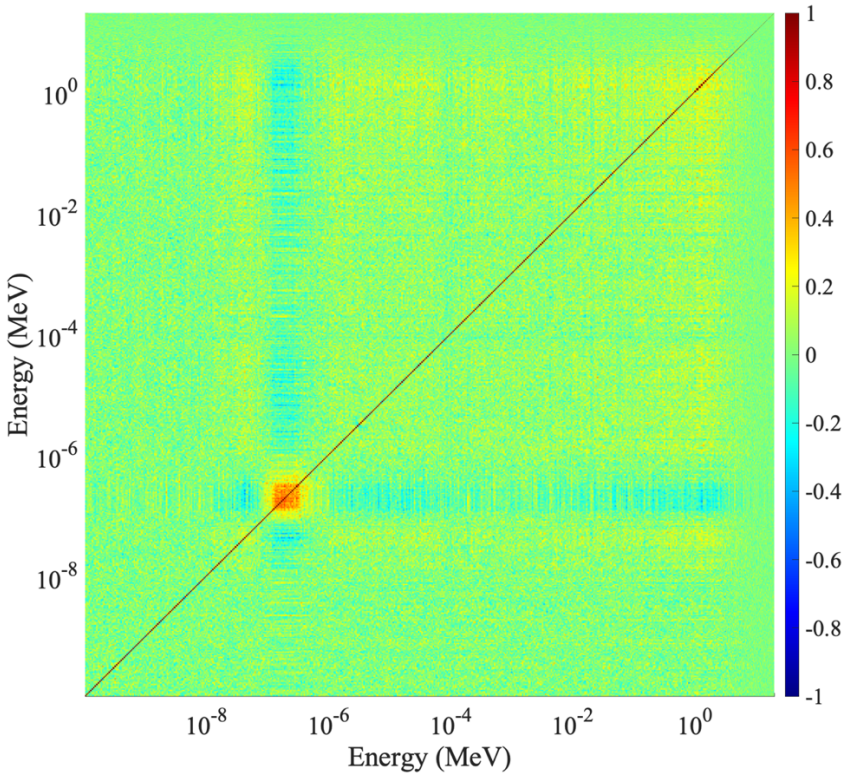

Figure 13. The correlation matrix for the 640-group neutron energy spectrum is based on the 110 multi-temp cases seen in this figure. The red sections show positive correlation in the thermal region, and possibly in the fast region. The light-blue regions show negative correlation, and they are expected in the matrix because correlation must be balanced. Many aspects of this correlation can be explained through the 6-factor formula (Equation (4)).

The results presented in Figure 12 and Figure 13 indicate that correlation observed in the previously assumed matrices in the thermal and fast regions may be partly attributed to fuel temperature variations. Uranium cross sections have been widely studied and present lower uncertainty than the other materials in the reactor, however, uranium cross section data still contributes significant uncertainty in some energy regions. Cross sections for the other materials in the reactor can be associated with higher uncertainties due to lack of cross section studies and experiments.

The correlation observed in the thermal region of Figure 13 can be interpreted through the components of the s*ix-factor formula* shown in Equation (4), where η is the reproduction factor, f is the thermal utilization factor, p is the probability a neutron will slow down from fission energy to thermal energies without being captured by a neutron resonance, ϵ is the fast fission factor, P_{FNL} is the probability a fast neutron will not leak, and P_{TNL} is the probability a thermal neutron will not leak.

$$k_{eff} = \eta\, f\, p\, \epsilon\, P_{FNL}\, P_{TNL} \tag{4}$$

The neutron cross sections (e.g., fission, capture, scattering) in the fuel rods will change as fuel temperature varies. In the ACRR MCNP model, an increase in fuel temperature produces a decrease in k_{eff}. The term η is calculated using the fuel fission and fuel absorption cross sections ($\eta = \nu\sigma_f^F/\sigma_a^F$), f uses both the fuel absorption cross section and the total absorption cross section in the reactor ($f = \Sigma_a^F/\Sigma_a$), and p is based on the resonance cross sections which are widened or narrowed by the doppler broadening effects.

The cross sections are used to determine the probabilities of neutrons interacting in the material based on neutron energy. The fuel temperature increase broadens the resonance capture

cross section which prevents some of the fast neutrons from reaching the thermal region, consequently lowering the fissions in the system. Due to decreased fissions, the neutron population moves to a subcritical system affecting the k_{eff}. This thermal relationship can be understood through f and η both of which rely on the absorption cross sections.

The fast neutron energy region reflects the neutrons born of fission. Fuel temperature variations were not expected to affect the fast neutron region. The negative correlation region shown in Figure 13 is expected due to the properties of a positive semi-definite correlation matrix, which requires a balance between positive and negative correlation for an overall sum of zero.

The negative correlation bands could represent the neutron energy equilibrium or slowing down that occurs in the negative direction balancing the neutron energies in the thermal region. If the neutrons continued to lose their energies indefinitely, eventually they would have no energy, but this does not happen. Once the neutrons down-scatter to thermal energies, the neutrons maintain neutron energy equilibrium by up-scattering or being absorbed. The neutron slowing down energy region effects are typically dominated by the effects to the moderator. No changes were made to the temperature of the moderator, so changes to p are not expected to occur.

After analyzing the MCNP 640-group neutron energy output, some regions were not sampled or were sampled so infrequently the uncertainty in those regions approached 100%. Figure 14 shows the fractional standard deviation of the sampling based on MCNP outputs at each energy group, which is compared to the fractional standard deviation of the data based on the Fluence per MJ at each energy group. The uncertainty in the spectrum increases significantly in the thermal region, mainly in the ‘cold neutron region’ below 0.025 eV, and the fast region

above 4 MeV. The fractional standard deviation of the data based on the Fluence per MJ at each energy group shows the regions for which there is unknown nuclear data [6].

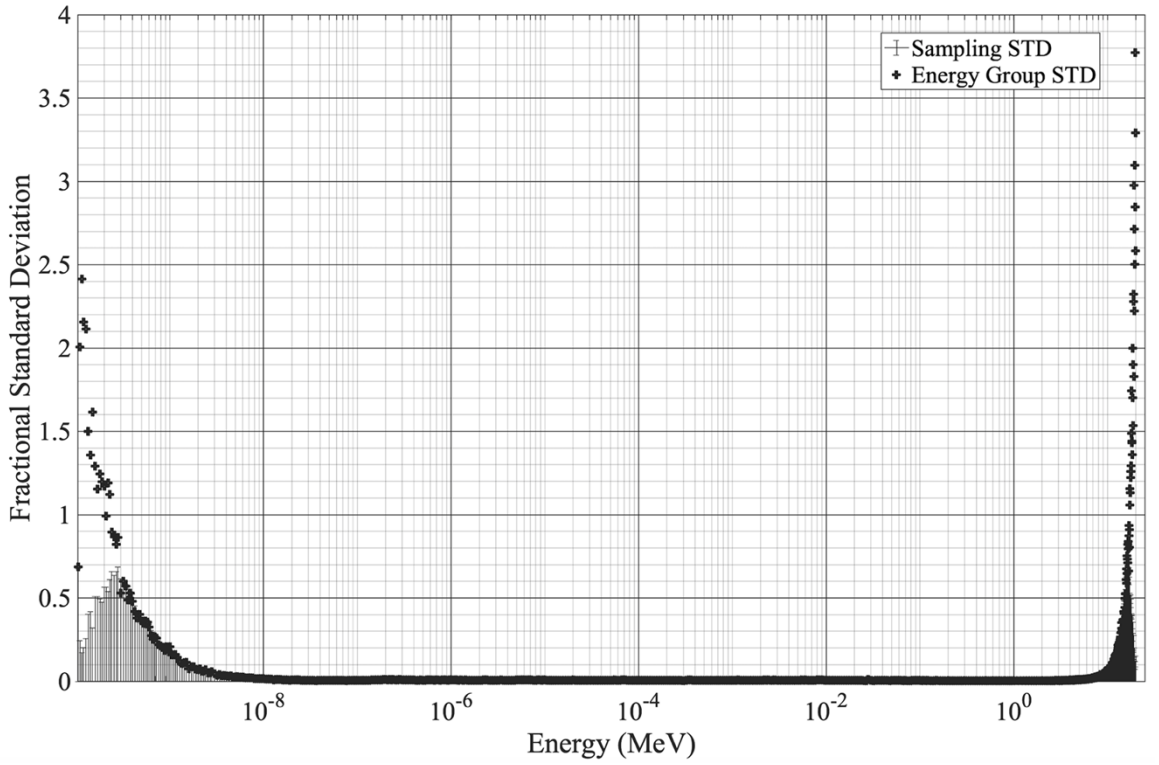

Figure 14. This plot shows the 640-group neutron energy fractional standard deviation of sampling and the fractional standard deviation of the nuclear data for all 110 cases. The black lines show sparse sampled regions based on MCNP in the 'cold neutron region' below 0.025 eV and fast neutron regions above 4 MeV. The plus symbols represent the fractional standard deviation of the data based on the Fluence per MJ and indicates the regions for which there is unknown nuclear data. This shows MCNP could not adequately sample the 'cold neutron region' and fast energy regions.

IV. CONCLUSION

Covariance and correlation matrices were built for the fuel temperature perturbations in the MCNP ACRR model, using the existing neutron libraries to evaluate the uncertainty propagation. The S(α,β) treatment was implemented to account for the low energy regions in the spectrum. Based on the results, some uncertainty from temperature variations in the fuel is a contributing factor to the uncertainty in the thermal neutron region. The correlations shown in the thermal and fast neutron energy regions coincided with the values in the previously assumed correlation matrix. There is a possibility fuel temperature variation within the fuel are not a dominant source of uncertainty. A source of uncertainty that may reflect in the previously assumed could be caused by other aspects of the ACRR MCNP model, like the moderating water temperature. Better resolution in the matrices can be achieved by increasing the number of particles or cycles per case. While this study only considered temperature variations in the fuel, potential future work includes investigating the impact of temperature variations in the water moderator in the ACRR MCNP model.

V. REFERENCES

[1] D. Redhouse, K. Curie and C. Peters, "An Energy Dependent Covariance Matrix of the Annular Core Research Reactor Fluence Using A Simplified Total Monte Carlo Technique," Technical Report SAND2019-11393A, 2019.

[2] M. Motamed, "math.unm.edu," Fall 2018. [Online]. Available: https://math.unm.edu/~motamed/UQ2018/intro.pdf. [Accessed 2021].

[3] Los Alamos National Laboratory, MCNP User's Manual Code Version 6.2, LA-UR-17-29981, 2017.

[4] J. G. Williams, D. W. Vehar and P. Griffin, "Covariance Matrices for Calculated Neutron Spectra and Measured Dosimeter Responses," Albuquerque, NM.

[5] J. R. Taylor, An Introduction to Error Analysis, Mill Valley: University Science Books, 1997.

[6] M. A. Moreno, *Monte Carlo Pertubation Analysis of Fuel Temperature Variations in the MCNP Model of the Annular Core Research Reactor,* Albuquerque: SAND2021-4556 T, 2021.

[7] E. J. Parma, G. E. Naranjo, R. M. Vega, L. L. Lippert, D. W. Vehar and P. J. Griffin, Radiation Characterization Summary: ACRR Central Cavity Free-Field Environment with the 32-Inch Pedestal at the Core Centerline (ACRR-FF-CC-32-cl), Technical Report SAND2015-6483, 2015.

[8] M. M. El Wakil, "Nuclear Heat Transport," American Nuclear Society, La Grange Park, 1978.

[9] K. R. DePriest, P. J. Cooper and E. J. Parma, "MCNP/MCNPX Model of the Annular Core Research Reactor," Technical Report SAND2006-3067, 2006.

[10] B. Rearden and M. Jessee, SCALE Code System, Oak Ridge: Oak Ridge National Laboratory, 2018.

[11] MathWorks Inc., "MATLAB: the Language of Technical Computing. Desktop Tools and Development Enviroment 7th ed," Math Works, Massachusetts, 2005.

[12] Python, "Python," 2020. [Online]. Available: https://docs.python.org/3/faq/general.html#what-is-python.

[13] D. G. Talley, "RAZORBACK – A Research Reactor Transient Analysis Code, Version 1.0," Sandia National Laboratories, Albuquerque, 2017.

[14] V. McLane and MCSEW, ENDF-201 ENDF/B-VI Summary Documentation

Suplement I, New York: NNDC BNL, 1996.

[15] S. Richards, "Stochastic mixing of bound thermal scattering data in MONK," *Annals of Nuclear Energy,* vol. 136, 2020.

[16] G. McKinney and J. C. Wagner, "MCNP/KENO Criticality Comparison," in *Proceedings of the Topical Meeting on Physics and Methods in Criticality Safety*, Nashville, 1993.

[17] J. Conlin, Listing of Available ACE Data Tables, LA-UR-17-20709, 2017.

[18] D. R. Redhouse, "Uncertainty Quantification of a Genetic Algorithm for Neutron Energy Spectrum Adjustment," SAND2017-4728T, College Station, 2017.

[19] M. Aufiero, A. Bidaud, D. Kotlyar, J. Leppänen, G. Palmiotti, M. Salvatores, S. Sen, E. Shwageraus and M. Fratoni, "New Approaches and Applications for Monte Carlo Perturbation Theory," in *International Conference on Mathematics & Computational Methods Applied to Nuclear Science & Engineering*, Jeju, 2017.

[20] J. L. Conlin, D. K. Parsons, S. J. Gardiner, A. C. I. Kahler, M. B. Lee, M. C. White and M. G. Gray, "Continuous Energy Neutron Cross Section Data Tables Based upon ENDF/B-VII.1 (LA-UR-13-20137)," Los Alamos National Laboratories, Los Alamos, 2013.